Low-strength lithosphere beneath the Ulleung Basin in the East Sea (Sea of Japan), inferred from buckling structure

Seok-Hyeon Do[1], Byung-Dal So[1], Young-Gyun Kim[2], and Gi-Bom Kim[3]

[1]Department of Geophysics, Kangwon National University, Chuncheon 24341, Republic of Korea

[2]Research Institute for Earth Resources, Kangwon National University, Chuncheon 24341, Republic of Korea

[3]Department of Geological Science, Pusan National University, Busan 46241, Republic of Korea.

Corresponding author: Byung-Dal So (bdso@kangwon.ac.kr)

Key Points:

- 2D viscoelastic basin modeling was performed to reproduce the buckling structure in the East Sea (Sea of Japan).
- The geometry of the buckling structure was more sensitive to the Moho temperature than the crustal type.
- Models with high Moho temperatures and low lithospheric strengths are consistent with the buckling structure observed in seismic profiles.

ABSTRACT

To understand back-arc basin dynamics of the western Pacific, constraining the crustal type and rheology of the Ulleung Basin in the East Sea (Sea of Japan) is essential. We performed finite element modeling using a wide range of rheology to analyze the buckling structures observed in the Ulleung Basin with wavelengths of ~60–70 km and amplitudes of ~150–200 m. When a high Moho temperature (i.e., 570–640 °C) was adopted, both the oceanic and continental crustal models exhibited surface topographies and heat flow values similar to those observed in the region. Furthermore, the line force of the models was <1.5 TN/m, which is considerably lower than the known value from plate boundaries. The results indicate that the lithosphere beneath the Ulleung Basin is weak. Thus, we argue that the East Sea does not fully support far-field tectonic stress propagation from the Japan Trench to the Korean Peninsula.

Plain Language Summary

The back-arc basin, which is closely related to subduction dynamics, acts as a stress transfer medium between plate boundaries and intraplate regions. Thus, estimation of lithospheric strength beneath a back-arc basin can provide insights into plate tectonics and intraplate seismicity. The East Sea (Sea of Japan), including the Ulleung Basin, is a back-arc basin between major plates (i.e., Pacific and Philippine Sea Plates) and the Korean Peninsula. To investigate the strength of the lithosphere beneath the East Sea, we modeled the observed compressional buckling topography in the Ulleung Basin. A thermal mechanical model was designed to analyze the effects of crustal type, Moho temperature, and brittle and ductile strength on the buckling geometry. We demonstrate the best-fit Moho temperature by constraining the geophysical observations, such as buckling geometry and marine heat flow data. When the Moho temperature was high, the buckling geometry of the Ulleung Basin was generated regardless of the crustal type. This weak lithosphere of the Ulleung Basin infers that the far-field stress from the Japan Trench is attenuated during long distance transmission. These findings suggest a need for further exploration of internal stress sources, such as gravitational potential energy, that may influence intraplate faults in southeastern Korea.

1 Introduction

The dynamics of back-arc basin evolution, related to far-field plate kinematics (Sdrolias & Müller, 2006), provide insights into the rheology of the lithosphere. The East Sea (Sea of Japan), located in the northeastern part of the western Pacific, is a mature back-arc basin, which was extended from the early Oligocene to the middle Miocene due to the retreat of the Japan Trench (Lallemand, S., & Jolivet, 1986; Sato et al., 2020). Since the late Miocene, the East Sea has been compressed by the advancing Japan Trench, the India–Eurasian collision, and the subduction of the Philippine Sea plate (Chough & Barg, 1987). Geodetic (Lee et al., 2011) and focal mechanism (Choi et al., 2012) studies have shown that the intraplate Korean Peninsula (KP) and the surrounding margins are under an E–W compressional regime, which is rotated slightly from the NW–SE advancing motion of the Japan Trench (Lee et al., 2017; Figure 1a and inset). Furthermore, sedimentary layers in the Ulleung Basin (UB) in the East Sea display apparent buckling structures with wavelengths of ~60–70 km and amplitudes of ~150–200 m (Kim et al., 2018[a], Figures 1b and 1c), indicating a compressional stress field.

The rheology of the lithosphere beneath the UB, which has a major effect on basin dynamics, is poorly constrained. The Thickened Oceanic Crust (TOC) and Extended Continental Crust (ECC) models have been used to explain the geophysical signatures of the UB, which has a thickness of ~10–15 km, thicker than normal oceanic crust (Itoh, 2001). The TOC model was proposed to explain the typical layers of oceanic crust in terms of their seismic velocity (Ludwig et al., 1975). The ECC model has also been adopted because linear geomagnetic anomalies have not been observed in the UB (Otofuji et al., 1985). In addition, previous studies have argued that the UB is hotter than other back-arc basins (e.g., Kim et al., 2016). Based on high marine heat flow (i.e., ~140 mW/m^2; Kim et al., 2010) and sedimentation rate (see Figures 1b and 1c), the calibrated heat flow value (Equation S1) is ~170 mW/m^2 (see Figure 1a).

When the lithosphere is under compression, the viscoelastic strength contrast within it may drive a folding instability, with various wavelengths and amplitudes (Cloetingh et al., 1999; Marques & Podladchikov, 2009). These lithospheric buckling structures are affected by the features of the brittle-ductile transition zones (BDTZ), such as depth, number, and strength, which vary widely depending on crustal rheology (Martinod & Davy, 1994). Previous numerical studies have attempted to simulate the buckling structures in the Himalayas and the Bay of Bengal, to estimate plate strength (Caporali, 2000; Gerbault, 2000). Thus, we can invert the rheology of the UB by investigating buckling structures and heat flow data.

In this study, we performed two-dimensional (2D) numerical modeling of viscoelastic rheology. The TOC and ECC models were applied using a wide range of Moho temperatures and rheological parameters to obtain buckling structures. We herein suggest the best-fit numerical models for the buckling structures observed in the seismic stratigraphy, then discuss the lithosphere strength of the UB and the implications for seismo-tectonics in SE Korea.

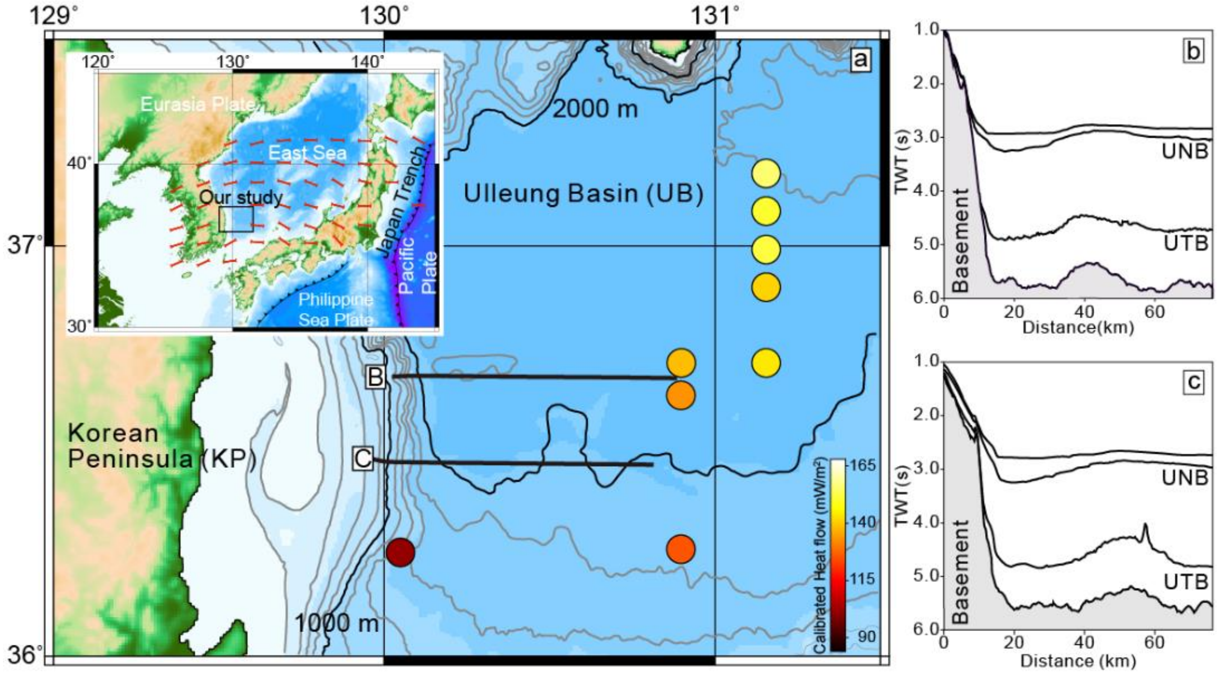

Figure 1. (a) Bathymetric map of the study area, showing the locations of calibrated heat flow measurements (circles) and seismic reflection profiles (thick black lines). Inset shows tectonic configuration, with major plates surrounding the KP and the UB. Red bars indicate the compressional stress direction (after Choi et al., 2012). Marine heat flow data (Kim et al., 2010) are calibrated using the sedimentation rate. (b) and (c) Interpretations of the seismic reflection profiles (after Kim et al., 2018[a]). UNB — Ulleung Neotectonic Boundary (ca. 3.8 Ma), and UTB — Ulleung Tectonic Boundary (ca. 12.5 Ma).

2 Numerical methods

We developed 2D Lagrangian viscoelastic models, using the TOC and ECC models, to investigate the compressional buckling structures observed in the UB. We used the finite element package, COMSOL Multiphysics®. The model domain of 640×100 km consisted of a 240×12 km basin (i.e., TOC or ECC), two 200×30 km continental crusts on either side, and underlying lithosphere (see Figures 2a and 2b). The continental crust surrounding the basin included a 20-km-long continent-ocean transition zone. We controlled the transition zone shape and basin depth, to satisfy the initial isostatic equilibrium below a depth of 30 km, representing the thickness of the continental crust. A single-layer oceanic crust was added to the basin for the TOC models (Lee et al., 1999) (Figure 2a), while two layers of continental crust (4 km of upper and 8 km of lower crusts) were assumed for the ECC models (Yoon et al., 2014) (Figure 2b). We imposed a constant compressional strain rate ($\dot{\varepsilon}_{bg} = 10^{-16}$ s^{-1}) on the side walls until 1% bulk shortening was achieved. The boundary conditions at the top and bottom of the model were defined as a free surface and free slip, respectively. To mimic the isostatic restoring force driven by lithospheric deformation (Lithgow-Bertelloni & Guynn, 2004; Choi et al., 2013), a boundary force was implemented along the initial compensation depth (see dashed lines in Figures 2a and 2b) as ρgv, where ρ, g, and v denote the density, gravitational acceleration, and vertical displacement along the dashed lines, respectively. Linear temperature profiles were adopted along the top (0 °C), Moho, and bottom (1350 °C) of the model. We varied the Moho temperature (T_M) from 350–650 °C.

We used a Maxwell viscoelastic material to constitute the stress-strain relationship (Equation 1).

$$\dot{\varepsilon}_{ij} = \dot{\varepsilon}_{ij}^{ela} + \dot{\varepsilon}_{ij}^{vis} \text{ where } \dot{\varepsilon}_{ij}^{ela} = \frac{1}{2G}\frac{D\tau_{ij}}{Dt} \text{ and } \dot{\varepsilon}_{ij}^{vis} = \frac{1}{2\eta_{eff}}\tau_{ij} \quad (1)$$

Here, $\dot{\varepsilon}_{ij}^{ela}$ and $\dot{\varepsilon}_{ij}^{vis}$ denote the elastic and viscous strain-rate, respectively. G and τ_{ij} are the shear modulus and the deviatoric stress tensor, while i and j indicate the horizontal and vertical directions, respectively. The effective viscosity (η_{eff}) was calculated using a composite rheology that follows the thermally activated dislocation creep (η_{dis}) and the pressure-dependent Moho–Coulomb ($\eta_{brittle}$) law (Equation 2).

$$\frac{1}{\eta_{eff}} = \frac{1}{\eta_{dis}} + \frac{1}{\eta_{brittle}} \text{ where } \eta_{dis} = f_s \cdot B \cdot \frac{1}{2A^{\frac{1}{n}}}\dot{\varepsilon}_{bg}^{\frac{1-n}{n}} exp\left(\frac{Q}{nRT}\right) \text{ and } \eta_{brittle} = \frac{Ptan\,\phi + C}{\dot{\varepsilon}_{bg}} \quad (2)$$

A, Q, n, B, P, and C refer to prefactor, activation energy, power-law exponent, material constant, lithostatic pressure, and cohesion, respectively. The ductile and brittle strengths were parameterized using a scale factor (f_s) and internal friction angle (ϕ) (e.g., Huismans & Beaumont, 2014). Details of the variables are listed in Table 1. The contrasts in viscosity and elastic shear modulus were simultaneously adopted following previous studies (e.g., Zhang et al, 1996; Damasceno et al., 2017). Thus, we applied the contrast in shear modulus to the model, which follows the contrast in viscosity. The reference shear modulus was 40 GPa for the continental crusts beyond the basin.

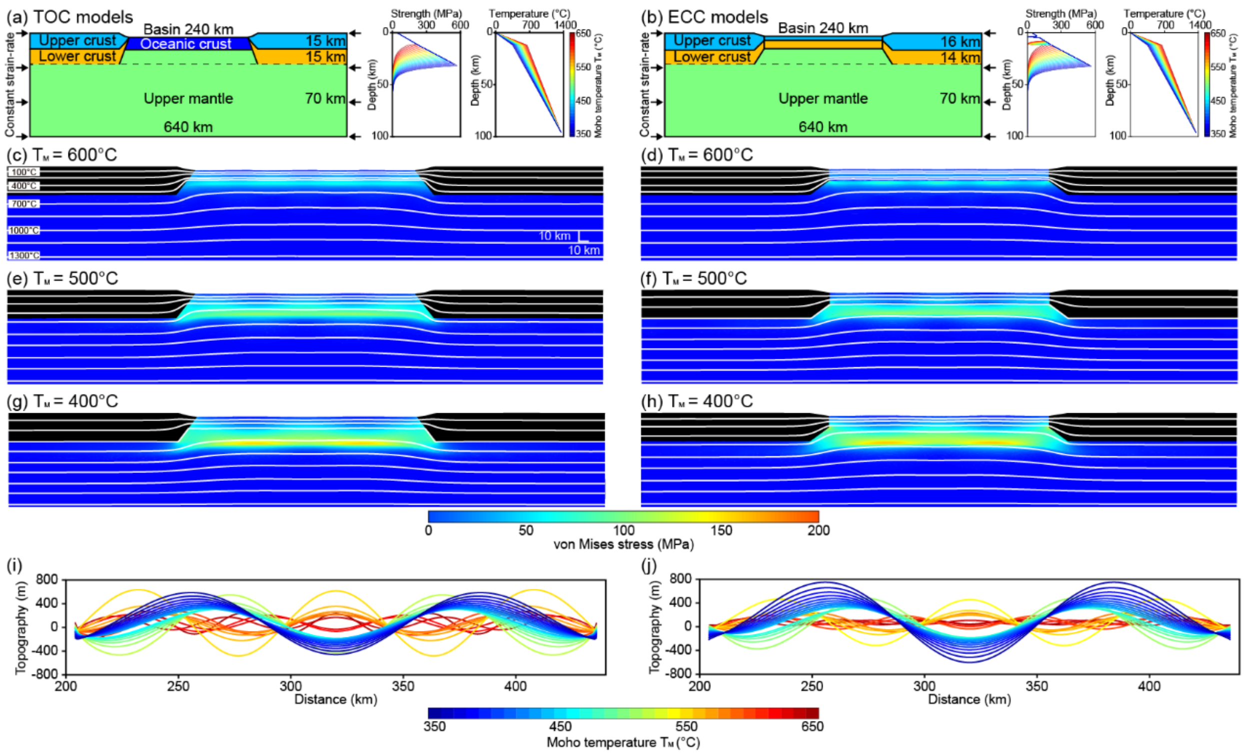

Figure 2. (a) and (b) Geometry and boundary conditions of the Thickened Oceanic Crust (TOC; left column) and Extended Continental Crust (ECC; right column) models. The blue, light blue, yellow, and green colors indicate oceanic crust, upper crust, lower crust, and mantle, respectively. The right boxes in (a) and (b) show the temperature and strength profiles for various Moho temperatures (T_m). (c)-(h) Distributions of von Mises stress. The white contours are isotherms. (i) and (j) Surface topographies with varying T_M.

Table 1. Values of parameters

	ρ [kg/^{3}]	A [Pa^{-n}s^{-1}]	Q [kJ/mol]	n	B	f_s	ϕ [°]	C [MPa]
Upper crust (wet quartz)	2700	1.1×10^{-28}	223	4	0.01	1, 1.4	15, 25	20
Lower crust (dry diabase)	2800	5.8×10^{-27}	485	4.7	0.02			
Oceanic crust (wet olivine)	3000	1.8×10^{-14}	430	3	3			
Upper mantle (wet olivine)	3300	1.8×10^{-14}	430	3	3			

*van Wijk & Blackman, 2005; Chenin &Beaumont, 2013; Huismans & Beaumont, 2014

3 Results

We conducted a series of numerical experiments to evaluate the effect of the Moho temperature on the formation of buckling structures, using the TOC and ECC reference models (f_s = 1 and ϕ = 15°). A colder mantle induced deeper stress localization associated with the buckling structures. The stress localization depth for T_M = 600 °C (Figure 2c) and T_M = 400 °C (Figure 2g) were ~15 km and ~30 km, respectively, which correspond to the depth of maximum strength, near the BDTZ. This implies that buckling is caused by a contrast in mechanical strength between the BDTZ and its surroundings. The TOC and ECC models with a warm mantle resulted in small surface wavelengths (λ_s) and amplitudes (A_s). The ranges of λ_s and A_s were ~60–70 km and ~100–200m, respectively, when T_M = 600 °C. For the models with a cold mantle (T_M = 400 °C), the values of λ_s and A_s were twice those of the warm mantle cases. Figures 2i and 2j show the surface topography of all reference TOC and ECC models, respectively, with T_M = 350–650 °C. The colors indicate T_M. Most of the warmer mantle cases show a smaller wavelength and amplitude than the colder mantle cases.

We analyzed the effects of T_M, ϕ, and f_s on the buckling geometry (i.e., λ_s and A_s) and stress level (i.e., average of line forces: f_L) in the TOC and ECC models (Figure 3). From the reference models, we changed the f_s and ϕ to 1.4 and 25°, respectively, to test the effects of lithospheric strength on buckling structure. The increases in f_s (plus symbols) and ϕ (cross symbols) indicate the increases in brittle and ductile strength, respectively. The largest strength is defined when both f_s and ϕ are increased (asterisk symbols). We compiled 100 TOC and 99 ECC models, excluding results with unrealistically large mesh distortions. We observed a negative linear correlation between λ_s and T_M (Figure 3a) from the results using different crustal types and various f_s and ϕ values, even though λ_s generally increases when the larger f_s and ϕ are values were adopted. The values of λ_s decreased from ~130 km to ~40 km when T_M increased from 350 °C to 650 °C. The left and right insets of Figure 3a exhibit the surface topographies of the reference cases with T_M = 350 °C and T_M = 650 °C, respectively. We confirm that the wavelength scales of the TOC (solid lines) and ECC (dashed lines) models are primarily determined by T_M. This implies that T_M, instead of crustal type, controls the buckling structure.

Although the values of A_s exhibit a relatively complex pattern, characterized by repeating U-shaped curves (Figure 3b), A_s decreases with increasing T_M. The U-shaped pattern of A_s can be attributed to dynamic buckling growth following a discrete buckling mode change with continuous viscoelastic stress relaxation. In the colder mantle models (T_M = 350–400 °C), A_s is highly variable (300–1200 m), depending on crustal type and lithospheric strength (i.e., f_s and ϕ). However, the range of A_s is narrow (~40–500 m) in the warm mantle models (T_M = 600–650 °C), indicating that the type of crust overlying a warm mantle has a small influence on the buckling amplitude. Figure 3c shows the averages of the line integrals along 13 evenly spaced stress profiles in the basin, denoted by f_L. A bimodal distribution dependent on ϕ (15 vs. 25 °) was observed in cold mantle cases. However, the f_L in warm mantle (T_M = 600–650 °C) with TOC and ECC models ranged from ~0.5 to 1.5 TN/m.

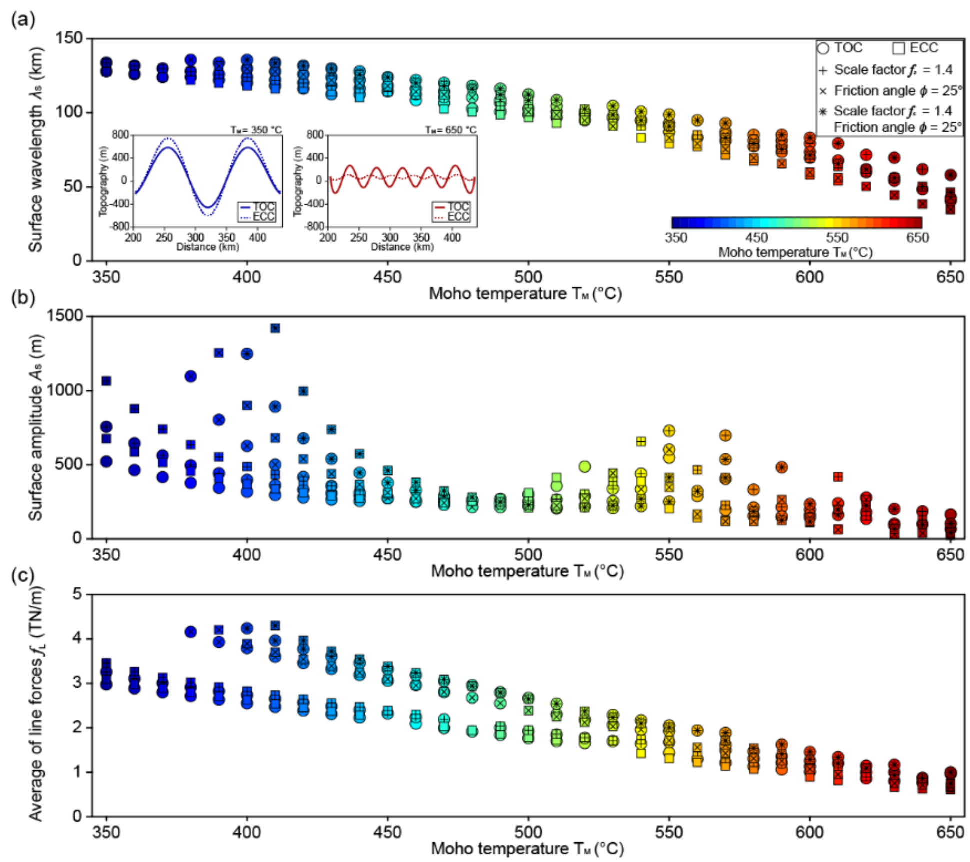

Figure 3. The variation in (a) surface wavelengths λ_s, (b) surface amplitudes A_s, and (c) average of line forces f_L with different Moho temperatures T_M and other variables, such as scale factor f_s and internal friction angle ϕ. The TOC and ECC models are denoted by circles and rectangles, respectively. Plus and cross symbols indicate the models with higher f_s (1.4) and ϕ (25°), respectively, than the reference model (i.e., f_s = 1 and ϕ = 15°). The asterisk symbols refer to models which had increases in both f_s and ϕ.

Figure 4a shows the relationship between λ_s and A_s with T_M (see colors). Overall, the values of λ_s and A_s decrease with increasing T_M, exhibiting a clear U-shaped pattern. The shaded areas indicate the ranges of λ_s (55–75 km) and A_s (125–225 m) for the buckling observed in the UB (Kim et al., 2018[a]). The buckling mode gradually changes with increasing T_M when a positive correlation between λ_s and A_s is observed. In contrast, a negative correlation leads to maintenance of the mode. Insets of Figure 4a display the surface topographies of the selected TOC models. The buckling mode increases with a decrease in A_s when T_M changes from 350 °C (blue line) to 460 °C (light blue line). With a further increase to 520 °C (green line), A_s increases while the mode is maintained. In models with higher T_M, a similar pattern is observed (see lower inset). The shaded area in Figure 4a includes 7 TOC (T_M = 590–640 °C) and 6 ECC (T_M= 570–620 °C) models with various f_s and ϕ values that are consistent with the buckling wavelength and amplitude observed in the UB. The TOC and ECC models with high T_M (570–640 °C) could explain the small buckling structures in the UB. Furthermore, the range of T_M in the shaded area corresponds to a heat flow of 161–181 mW/m^2 at the crust top (Figure 4b) assuming a thermal conductivity of 3.4 W/(m·K), which matches the calibrated marine heat flow data by eliminating sedimentation effect in the UB.

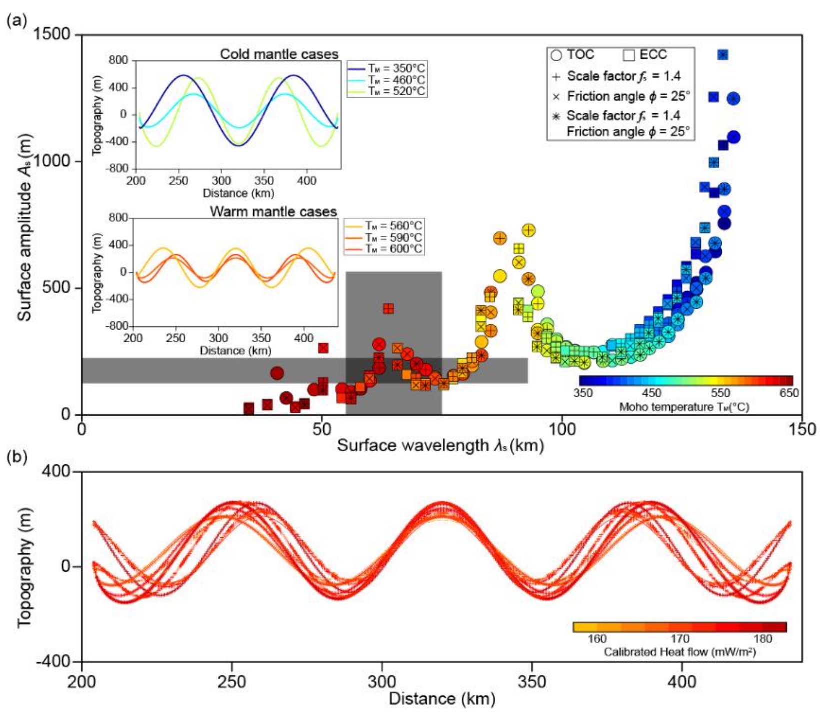

Figure 4. The relationship between λ_s and A_s with various variables (i.e., f_s and ϕ) and a varying T_M. Vertical and horizontal shaded areas indicate the ranges of λ_s (55–75 km) and A_s

(125–225 m), respectively, for the buckling observed in the UB. Insets show surface topography with varying T_M to explain the change in buckling mode. Upper and lower insets illustrate the cold and warm mantle cases, respectively. (b) Comparison between the surface topographies (colored lines) of the TOC and ECC models in the shaded area in (a). The color indicates the values of surface heat flow.

4 Discussion

In this study, we found that the buckling geometry observed in the UB formed with Moho temperatures as high as 570–640 °C, regardless of the crust type (i.e., both TOC and ECC models). The consistency of the numerical results combined with seismic profiles (Kim et al., 2018[a]) of the buckling geometry (i.e., wavelength and amplitude) and marine heat flow data (Kim et al., 2010), indicate that the lithosphere beneath the UB is warm and weak compared to normal oceanic crust. Our finding is compatible with the knowledge that back-arc basin crust is inherently different to normal oceanic crust due to the presence of depleted mantle in subduction zones (Grevemeyer et al., 2020).

We found that larger strength contrasts (i.e., lower Moho temperatures) produce buckling structures with larger wavelengths and amplitudes. However, a retrograde pattern, in which a higher Moho temperature yields a larger amplitude, is observed at specific conditions. Previous buckling studies (e.g., Zhang et al., 1996) using ideal settings, such as vertically fixed top boundary and discretely layered strengths, have shown that the amplitude and wavelength increase monotonically with an increasing strength contrast. This discrepancy stems from the free top boundary and the brittle-ductile rheology, depending on temperature and pressure, which are required for realistic modeling of buckling.

The buckling structures in the UB, with their complex tectonic histories, may have been affected by shear heating, hot mantle upwelling (Kim & So, 2020), and sedimentary loading. Shear heating with inelastic deformation, which dramatically reduces the lithospheric strength, may promote a highly localized ductile thrust during the growth of the buckling structure (Schmalholz et al., 2009). Thus, we consider that the shear heating effect might be negligible, because the UB buckling is quasi-periodic. Furthermore, shear heating is less vigorous under high temperature conditions (So & Yuen 2014), corresponding to the warm mantle beneath the East Sea.

Mantle upwelling beneath the East Sea, supported by volcanic islands (Lee & Suk, 1998) and a low seismic velocity anomaly in the mantle (Ismail-Zadeh et al., 2013), can be explained by either Big Mantle Wedge (Zhao et al., 2009) or Edge-Driven Convection (Choi, 2020). However, considering the large timescale differences between fast elastic buckling growth and slow metasomatism of the lithosphere by a hot mantle (Harry & Leeman, 1995), we argue that mantle upwelling has only a minor effect on the growth of compressional buckling.

Localized vertical loading from thick sediment on the continental–oceanic boundary could induce a flexural bulge in the crust (Pazzaglia & Gardner, 1994). Although the UB is covered by ~4 km of sediment (Gnibidenko, 1979), each uniformly thick sediment layer older than 3.8 Ma shows a buckling geometry similar to that of the basement (see Figure 1b). The vertical-line loading from the sediment is rather non-differential. Therefore, we suggest that the main driving force of buckling in the UB is far-field compressional stress, possibly from the trench.

We found that in the models consistent with buckling in the UB, the integrated stress along the vertical profiles is ~0.8–1.3 TN/m, which is considerably lower than stresses along major plate boundaries (2.5–3 TN/m; Copley et al., 2010). This indicates that the UB buckling formed under low compressional stress and that far-field stress from the Japan Trench is attenuated during long distance propagation across other large basins and plateau. The far-field stress can be shared and rotated by the multiple faults, damaged zones, and mountain belts of intraplate regions (e.g., van der Pluijm et al., 1997). The World Stress Map revealed that the stress orientation of certain regions is different from that of plate boundaries (Heidbach et al., 2018). Similarly, there is a slight misfit between the advancing direction of the Japan Trench (NW–SE) and the stress field orientation (E–W) in the UB. Recent geodetic measurements have also suggested a prominent strain localization in SE Korea, which may be caused by crustal thickness differences (Kim et al., 2018[b]). Furthermore, Kim et al. (2018[a]) reported that strain localization along the major west-dipping thrust along the margin of SE Korea may cause mechanical decoupling of the UB and KP. Thus, we argue that the weak UB lithosphere is a poor stress guide for transmitting far-field stresses (So & Capitanio, 2017) to the KP from plate boundaries, which inspires us to further explore the intraplate stress sources of SE Korea.

Our study, by revealing the low strength of the UB between the Japan Trench and the KP, can provide insights into the mechanisms driving intraplate earthquakes in SE Korea. Although the KP is located far from the plate boundary, moderate earthquakes have occurred in this region, such as the 2016 M_w 5.6 Gyeongju and 2017 M_w 5.5 Pohang earthquakes (Chai et al., 2020). Internal factors such as the gravitational potential energy (GPE) difference from the horizontal elevation (Schmalholz et al., 2014) and density contrast (Levandowski et al., 2017) have been suggested as stress sources for intraplate faults. To understand the seismo-tectonics of the KP, precise quantifications of the relative contributions of far-field tectonic stresses (e.g., trench motion and continental collision) and internal factors (e.g., GPE) are required. Either the topography differences along the continental–oceanic boundary and/or dense mafic body beneath the crust (Cho et al., 2004; Kim et al., 2017) in SE Korea could be a source of stress for intraplate faults.

5 Conclusions

We performed 2D viscoelastic Lagrangian numerical modeling to investigate the buckling structures and rheology of the UB. The conclusions of this study are as follows:

(1) When a warmer mantle (i.e., higher T_M) is adopted, buckling structures with smaller λ_s and A_s values are generally shown.

(2) Regardless of the crustal type (i.e., TOC or ECC) and rheological parameters (i.e., f_s and ϕ) controlling brittle and ductile strengths, buckling structures similar to those in the UB are obtained using a warm mantle (T_M > 570 °C).

(3) Based on the numerical results constraining the observed buckling in the UB and marine heat flow data, we suggest that the rheology beneath the UB is weak.

(4) The weak UB may not fully accommodate the stress propagated from the Japan Trench to the KP, which may indicate another stress source for intraplate faults in SE Korea.

Acknowledgments and Data Availability Statement

This research was supported by the National Research Foundation of Korea (NRF-2019R1C1C1010804 and No. 2019R1A6A1A03033167) grant that was awarded to B.-D. So. S.-H. Do was supported by the Ministry of the Interior and Safety, as the Human Resource Development Project in Disaster Management. Y.-G. Kim was supported by the National Research Foundation of Korea (No. 2020R1C1C1007495). Model input and movie files for our numerical modeling can be downloaded using the link: https://zenodo.org/record/4447022.

References

Caporali, A. (2000). Buckling of the lithosphere in western Himalaya: Constraints from gravity and topography data. Journal of Geophysical Research: Solid Earth, 105, 3103-3113. doi:https://doi.org/10.1029/1999JB900389

Chai, G., Yoo, S., Rhie, J., & Kang, T. (2020). Stress-Drop Scaling of the 2016 Gyeongju and 2017 Pohang Earthquake Sequences Using Coda-Based Methods. Bulletin of the Seismological Society of America, 110(5), 2047-2057. doi:10.1785/0120200132

Chenin, P., & Beaumont, C. (2013). Influence of offset weak zones on the development of rift basins: Activation and abandonment during continental extension and breakup. Journal of Geophysical Research: Solid Earth, 118(4), 1698-1720. doi:https://doi.org/10.1002/jgrb.50138

Cho, H., Kim, H., Jou, H., Hong, J., & Baag, C. (2004). Transition from rifted continental to oceanic crust at the southeastern Korean margin in the East Sea (Japan Sea). Geophysical Research Letters, 31(7) doi:https://doi.org/10.1029/2003GL019107

Choi, H., Hong, T., He, X., & Baag, C. (2012). Seismic evidence for reverse activation of a paleo-rifting system in the East Sea (Sea of Japan). Tectonophysics; Seismic Imaging of Continents and their Margins: New Research at the Confluence of Active and Passive Seismology, 572-573, 123-133. doi:https://doi.org/10.1016/j.tecto.2011.12.023

Choi, E., Buck, W. R., Lavier, L. L., & Petersen, K. D. (2013). Using core complex geometry to constrain fault strength. Geophysical Research Letters, 40(15), 3863-3867. doi:https://doi.org/10.1002/grl.50732

Choi, S. H. (2020). Geochemistry and petrogenesis of Quaternary volcanic rocks from Ulleung Island, South Korea. Lithos, , 105874. doi:https://doi.org/10.1016/j.lithos.2020.105874

Chough, S. K., & Barg, E. (1987). Tectonic history of Ulleung basin margin, East Sea (Sea of Japan). Geology, 15(1), 45-48. doi:10.1130/0091-7613(1987)15<45:THOUBM>2.0.CO;2

Cloetingh, S., Burov, E., & Poliakov, A. (1999). Lithosphere folding: Primary response to compression? (from central Asia to Paris basin). Tectonics, 18(6), 1064-1083. doi:https://doi.org/10.1029/1999TC900040

Copley, A., Avouac, J., & Royer, J. (2010). India-Asia collision and the Cenozoic slowdown of the Indian plate: Implications for the forces driving plate motions. Journal of Geophysical Research: Solid Earth, 115 doi:https://doi.org/10.1029/2009JB006634

Damasceno, D. R., Eckert, A., & Liu, X. (2017). Flexural-slip during visco-elastic buckle folding. Journal of Structural Geology, 100, 62-76. doi:https://doi.org/10.1016/j.jsg.2017.05.007

Gerbault, M. (2000). At what stress level is the central Indian Ocean lithosphere buckling? Earth and Planetary Science Letters, 178(1), 165-181. doi:https://doi.org/10.1016/S0012-821X(00)00054-6

Gnibidenko, H. (1979). The tectonics of the Japan Sea. Marine Geology, 32(1), 71-87. doi:https://doi.org/10.1016/0025-3227(79)90147-6

Grevemeyer, I., Kodaira, S., Fujie, G., & Takahashi, N. (2020). Structure of oceanic crust in back-arc basins modulated by mantle source heterogeneity. Geology, doi:10.1130/G48407.1

Harry, D. L., & Leeman, W. P. (1995). Partial melting of melt metasomatized subcontinental mantle and the magma source potential of the lower lithosphere. Journal of Geophysical Research: Solid Earth, 100, 10255-10269. doi:https://doi.org/10.1029/94JB03065

Heidbach, O., Rajabi, M., Cui, X., Fuchs, K., Müller, B., Reinecker, J., . . . Zoback, M. (2018). The World Stress Map database release 2016: Crustal stress pattern across scales. Tectonophysics, 744, 484-498. doi:https://doi.org/10.1016/j.tecto.2018.07.007

Huismans, R. S., & Beaumont, C. (2014). Rifted continental margins: The case for depth-dependent extension. Earth and Planetary Science Letters, 407, 148-162. doi:https://doi.org/10.1016/j.epsl.2014.09.032

Ismail-Zadeh, A., Honda, S., & Tsepelev, I. (2013). Linking mantle upwelling with the lithosphere descent and the Japan Sea evolution: a hypothesis. Scientific Reports, 3(1), 1137. doi:10.1038/srep01137

Itoh, Y. (2001). A Miocene pull-apart deformation zone at the western margin of the Japan Sea back-arc basin: implications for the back-arc opening mode. Tectonophysics, 334(3), 235-244. doi:https://doi.org/10.1016/S0040-1951(01)00068-3

Kim, D., & So, B.-D. (2020). Effects of rheology and mantle temperature structure on edge-driven convection: Implications for partial melting and dynamic topography. Physics of the Earth and Planetary Interiors, 303, 106487. doi:https://doi.org/10.1016/j.pepi.2020.106487

Kim, G., Yoon, S., Kim, S., & So, B. (2018). Transition from buckling to subduction on strike-slip continental margins: Evidence from the East Sea (Japan Sea). Geology, 46(7), 603-606. doi:10.1130/G40305.1

Kim, K., Park, J., Park, Y., Hao, T., & Kim, H. (2017). Crustal structure beneath the southern Korean Peninsula from local earthquakes. Geophysical Journal International, 209(2), 969-978. doi:10.1093/gji/ggx079

Kim, S., Tkalčić, H., Rhie, J., & Chen, Y. (2016). Intraplate volcanism controlled by back-arc and continental structures in NE Asia inferred from transdimensional Bayesian ambient noise tomography. Geophysical Research Letters, 43(16), 8390-8398. doi:https://doi.org/10.1002/2016GL069483

Kim, S., Ree, J., Yoon, H. S., Choi, B., & Park, P. (2018). Crustal Deformation of South Korea After the Tohoku-Oki Earthquake: Deformation Heterogeneity and Seismic Activity. Tectonics, 37(8), 2389-2403. doi:https://doi.org/10.1029/2018TC004967

Kim, Y., Lee, S., & Matsubayashi, O. (2010). New heat flow measurements in the Ulleung Basin, East Sea (Sea of Japan): relationship to local BSR depth, and implications for regional heat flow distribution. Geo-Marine Letters, 30(6), 595-603.

Lee, G. H., Kim, H. J., Suh, M. C., & Hong, J. K. (1999). Crustal structure, volcanism, and opening mode of the Ulleung Basin, East Sea (Sea of Japan). Tectonophysics, 308(4), 503-525. doi:https://doi.org/10.1016/S0040-1951(99)00113-4

Lee, G. H., Yoon, Y., Nam, B. H., Lim, H., Kim, Y., Kim, H. J., & Lee, K. (2011). Structural evolution of the southwestern margin of the Ulleung Basin, East Sea (Japan Sea) and tectonic implications. Tectonophysics, 502(3), 293-307. doi:https://doi.org/10.1016/j.tecto.2011.01.015

Lee, G. H., & Suk, B. (1998). Latest Neogene–Quaternary seismic stratigraphy of the Ulleung Basin, East Sea (Sea of Japan). Marine Geology, 146(1), 205-224. doi:https://doi.org/10.1016/S0025-3227(97)00123-0

Lee, J., Hong, T., & Chang, C. (2017). Crustal stress field perturbations in the continental margin around the Korean Peninsula and Japanese islands. Tectonophysics, 718, 140-149. doi:https://doi.org/10.1016/j.tecto.2017.08.003

Lallemand, S., & Jolivet, L. (1986). Japan Sea: a pull-apart basin? Earth and Planetary Science Letters, 76(3), 375-389. doi:https://doi.org/10.1016/0012-821X(86)90088-9

Levandowski, W., Zellman, M., & Briggs, R. (2017). Gravitational body forces focus North American intraplate earthquakes. Nature Communications, 8(1), 14314. doi:10.1038/ncomms14314

Lithgow-Bertelloni, C., & Guynn, J. H. (2004). Origin of the lithospheric stress field. Journal of Geophysical Research: Solid Earth, 109 doi:https://doi.org/10.1029/2003JB002467

Ludwig, W. J., Murauchi, S., & Houtz, R. E. (1975). Sediments and Structure of the Japan Sea. GSA Bulletin, 86(5), 651-664. doi:10.1130/0016-7606(1975)86<651:SASOTJ>2.0.CO;2

Marques, F. O., & Podladchikov, Y. Y. (2009). A thin elastic core can control large-scale patterns of lithosphere shortening. Earth and Planetary Science Letters, 277(1), 80-85. doi:https://doi.org/10.1016/j.epsl.2008.10.009

Martinod, J., & Davy, P. (1994). Periodic instabilities during compression of the lithosphere: 2. Analogue experiments. Journal of Geophysical Research: Solid Earth, 99, 12057-12069. doi:https://doi.org/10.1029/93JB03599

Otofuji, Y., Matsuda, T., & Nohda, S. (1985). Opening mode of the Japan Sea inferred from the palaeomagnetism of the Japan Arc. Nature, 317(6038), 603-604. doi:10.1038/317603a0

Pazzaglia, F. J., & Gardner, T. W. (1994). Late Cenozoic flexural deformation of the middle US Atlantic passive margin. Journal of Geophysical Research: Solid Earth, 99(B6), 12143-12157.

Sato, T., No, T., Arai, R., Miura, S., & Kodaira, S. (2020). Transition from continental rift to back-arc basin in the southern Japan Sea deduced from seismic velocity structures. Geophysical Journal International, 221(1), 722-739. doi:10.1093/gji/ggaa006

Schmalholz, S. M., Medvedev, S., Lechmann, S. M., & Podladchikov, Y. (2014). Relationship between tectonic overpressure, deviatoric stress, driving force, isostasy and gravitational potential energy. Geophysical Journal International, 197(2), 680-696. doi:10.1093/gji/ggu040

Schmalholz, S. M., Kaus, B. J., & Burg, J. (2009). Stress-strength relationship in the lithosphere during continental collision. Geology, 37(9), 775-778.

Sdrolias, M., & Müller, R. D. (2006). Controls on back-arc basin formation. Geochemistry, Geophysics, Geosystems, 7(4) doi:https://doi.org/10.1029/2005GC001090

So, B.-D., & Yuen, D. A. (2014). Stationary points in activation energy for heat dissipated with a power law temperature-dependent viscoelastoplastic rheology. Geophysical Research Letters, 41(14), 4953-4960. doi:https://doi.org/10.1002/2014GL060713

So, B.-D., & Capitanio, F. A. (2017). The effect of plate-scale rheology and plate interactions on intraplate seismicity. Earth and Planetary Science Letters, 478, 121-131. doi:https://doi.org/10.1016/j.epsl.2017.08.020

van der Pluijm, Ben A., Craddock, J. P., Graham, B. R., & Harris, J. H. (1997). Paleostress in Cratonic North America: Implications for Deformation of Continental Interiors. Science, 277(5327), 794-796. doi:10.1126/science.277.5327.794

van Wijk, J. W., & Blackman, D. K. (2005). Deformation of oceanic lithosphere near slow-spreading ridge discontinuities. Tectonophysics, 407(3), 211-225. doi:https://doi.org/10.1016/j.tecto.2005.08.009

Yoon, S. H., Sohn, Y. K., & Chough, S. K. (2014). Tectonic, sedimentary, and volcanic evolution of a back-arc basin in the East Sea (Sea of Japan). Marine Geology, 352, 70-88. doi:https://doi.org/10.1016/j.margeo.2014.03.004

Zhang, Y., Hobbs, B. E., Ord, A., & Mühlhaus, H. B. (1996). Computer simulation of single-layer buckling. Journal of Structural Geology, 18(5), 643-655. doi:https://doi.org/10.1016/S0191-8141(96)80030-7

Zhao, D., Tian, Y., Lei, J., Liu, L., & Zheng, S. (2009). Seismic image and origin of the Changbai intraplate volcano in East Asia: Role of big mantle wedge above the stagnant Pacific slab. Physics of the Earth and Planetary Interiors, 173(3), 197-206. doi:https://doi.org/10.1016/j.pepi.2008.11.009